



ESA CONTRACT REPORT

Contract Report to the European Space Agency

*Support-to-Science-Element (STSE) Study
EarthCARE Assimilation*

**WP-2100 report: Monitoring of radar
data**

January 2013, updated February 2014

*Authors: S. Di Michele, E. Martins,
M. Janisková*

ESA ESTEC contract 4000102816/11/NL/CT

**European Centre for Medium-Range Weather Forecasts
Europäisches Zentrum für mittelfristige Wettervorhersage
Centre européen pour les prévisions météorologiques à moyen terme**



ECMWF

Series: ECMWF ESA Project Report Series

A full list of ECMWF Publications can be found on our web site under:

<http://www.ecmwf.int/publications/>

Contact: library@ecmwf.int

©Copyright 2014

European Centre for Medium Range Weather Forecasts
Shinfield Park, Reading, RG2 9AX, England

Literary and scientific copyrights belong to ECMWF and are reserved in all countries. This publication is not to be reprinted or translated in whole or in part without the written permission of the Director-General. Appropriate non-commercial use will normally be granted under the condition that reference is made to ECMWF.

The information within this publication is given in good faith and considered to be true, but ECMWF accepts no liability for error, omission and for loss or damage arising from its use.

Contract Report to the European Space Agency

*Support-to-Science-Element (STSE) Study EarthCARE
Assimilation*

WP-2100 report: Monitoring of radar data

*Authors: S. Di Michele, E. Martins,
M. Janisková*

ESA ESTEC contract 4000102816/11/NL/CT

January 2013, updated February 2014

ABSTRACT

A basic framework for monitoring time series of radar observations has been established. Observations from CloudSat have been compared to the corresponding reflectivity first guess departures simulated from the ECMWF model. Our analysis shows that comparison with the model enables the detection of much smaller anomalies than monitoring observations alone. The study has also shown that cloud-top height derived from reflectivity is an appropriate diagnostic to monitor the instrument. Results suggest that instrument/model problems can be identified by monitoring the time series of first guess departures provided that the anomalies are outside their typical range of variation. For this purpose, a set of threshold values are defined, on which a warning system could be based.

Contents

1	Introduction	1
2	Monitoring of radar reflectivity	1
2.1	Time series of CloudSat reflectivity	2
2.2	Time series of CloudSat reflectivity FG departures	7
3	Monitoring of cloud-top height	14
3.1	Time series of cloud-top height from CloudSat	14
3.2	Time series of cloud-top height departures	15
4	Conclusions	20

1 Introduction

The future satellite mission, Earth, Clouds, Aerosols and Radiation Explorer (EarthCARE), is planned to use a combination of a lidar and a cloud radar to provide the vertical structure and the horizontal distribution of cloud and aerosol over all climate zones. Thanks to the CloudSat ([Stephens et al., 2002](#)) and CALIPSO ([Winker et al., 2009](#)) missions, coincident space-borne lidar and radar observations are already available providing good source of data for feasibility studies in preparation for the future EarthCARE mission. In the past, the ESA-funded project Quantitative Assessment of the Operational Value of Space-Borne Radar and Lidar Measurements of Cloud and Aerosol Profiles (QuARL, [Janisková et al., 2010](#)) carried at European Centre for Medium Range Weather Forecasts (ECMWF) has shown that such observations have the potential to be assimilated into Numerical Weather Prediction (NWP) models to improve their initial atmospheric state. In order to prepare for the exploitation of radar and lidar observations in data assimilation in the time frame of the EarthCARE mission, objective of the current study (STSE EarthCARE assimilation) is the development of an off-line system to monitor/assimilate Level-1 data from the CloudSat radar and the CALIPSO lidar in clouds within the global model run at ECMWF.

The monitoring of observational data is a fundamental element of all operational NWP centre data assimilation systems and the check of the model-vs-observation statistics is a necessary step before the active assimilation of new data can take place. Every new observation that is brought into the operational analysis system at ECMWF is first monitored for a period of time. This information also provides a unique tool to routinely check for instrument deficiencies using the model as a reference point. As first explained by [Hollingsworth et al. \(1986\)](#), there is good evidence that the 6-hour forecast error (first-guess error) is quite low, therefore allowing the evaluation of the data quality by comparison with the first-guess. Tracking departures and bias corrections, the monitoring activity helps to identify problems that may be affecting the observations (and/or the model). The complementary usage of many different observations in the system permits to separate between model issues and issues in the observations, for example, related to instrument deterioration. Research satellites can also benefit for a monitoring activity: recently [Muñoz Sabater et al. \(2012\)](#) used the ECMWF NWP model to assess the performance of the Soil Moisture and Ocean Salinity (SMOS) mission.

This report summarizes the results of monitoring CloudSat data within the ECMWF system, work done in the context of WP-2100 of the STSE EarthCARE study. First, in Section 2 the temporal evolution of CloudSat observations is described, considering both stand-alone reflectivities, and first guess (FG) departures (differences between observations and model equivalents). In Section 3, the feasibility of monitoring cloud-top height derived from reflectivity observations is then investigated. Conclusions from this monitoring study are provided in Section 4.

2 Monitoring of radar reflectivity

In this section, time series of CloudSat reflectivity and FG departures from the ECMWF short-term forecasts have been evaluated using the ZmVar radar operator ([Di Michele et al., 2012](#)), which updated version was described in WP-1100 [Di Michele et al. \(2014\)](#). By comparing the range of variation of their temporal evolution it is possible to understand whether there is any potential in routinely monitoring CloudSat observation against the corresponding quantities derived from a forecast model.

The study is based on the monitoring of time series of selected statistics (i.e. mean, standard deviation, number of observations) derived from the CloudSat data. In particular, the analysis is focused on a period of 30 days (January 2007). Different lengths are considered for the time window used to build the statistics: a single orbit (or granule), 12 hours (corresponding to the ECMWF 4D-Var assimilation window), 24 hours and a running average over a week (with a one-day stepping). This can show the sensitivity of the temporal evolution to the

size of the accumulation period. The monitoring task is usually performed separating the observations over different latitude belts in order to take into account the different meteorological regimes, which in turn reflect in different ranges of variation for observations. In this study, the investigation is done distinguishing between tropical (from 30°S to 30°N) and mid-latitude cases (below 30°S and above 30°N). For the latter, we will focus on cases in the Southern hemisphere (from 60°S to 30°S), since more observations are there available over ocean than when considering mid-latitude cases in the Northern hemisphere.

Statistics have been obtained using all available data over the ocean, screening for cases where the (in-cloud) values of liquid and solid convective precipitation prescribed by the IFS model are respectively larger than 0.03 and 3.0 g/m³. This condition corresponds to removing cases likely to be affected by multiple scattering (Section 2.5 of WP-1100 report, Di Michele et al., 2014).

2.1 Time series of CloudSat reflectivity

The temporal evolution of the mean reflectivity \bar{Z}_{CS} for CloudSat observations at Southern mid-latitudes is shown in Fig. 2.1. Each line corresponds to one of the chosen averaging time-windows. Results are given for six reference altitude levels, plotted in six separate panels where height decreases from top to bottom. Regardless of the vertical level, the main feature is the continual oscillation of the mean reflectivity from one time step to the next. As expected, the variations are most pronounced at granule level (minimum and maximum are reported in the title of each panel) and they decrease as the averaging time-window increases. One can notice that the range of variation gets to values much lower than the actual mean only performing at least a 24-hour averaging. Comparison across panels reveals that CloudSat mean reflectivity increases as the altitude decreases, with the most significant increment occurring going from 8 to 6 kilometres. Similar plots for CloudSat observations in the tropical region are displayed in Figure 2.2. Comparing with the mid-latitude case, we note a significant increase in the mean reflectivity above 6 km (because of more intense and towering cloud structures) and a decrease below 2 km (because of stronger signal attenuation), both justifying the separation between the two meteorological regimes.

The range of variation $\Delta\bar{Z}_{CS}$, defined as the difference between the maximum value and the minimum value of \bar{Z}_{CS} along the month, is given in Tab. 2.1 for each of the six reference levels under consideration. The table confirms, in a quantitative way, the beneficial effect of the averaging and the larger signal oscillations at the tropics.

The variability of CloudSat reflectivity within each averaging time window is expressed by the standard deviation $\sigma_{Z_{CS}}$. Figure 2.3 and Fig. 2.4 show time series of standard deviation for observations at Southern mid-latitudes and tropics, respectively. Table 2.2 gives the corresponding range of variation $\Delta\sigma_{Z_{CS}}$, which, similarly to the mean, is defined as the difference between the maximum and the minimum values of $\sigma_{Z_{CS}}$ in the month.

Another important quantity to consider is the number of CloudSat observations n_{CS} used to build the mean and standard deviation of reflectivity. It is worth mentioning that, since observations are averaged at the horizontal resolution of the IFS model, in order to be able to evaluate departures, these numbers are about 30 times smaller than the actual CloudSat measurements. The temporal evolution of n_{CS} is shown in Fig. 2.5. As expected, since the radar signal is mainly sensitive to precipitating ice and rain, the sample size decreases as altitude increases. It can also be noticed that, at all levels, the sample size stays quite stable along the month-long test period. However, this is not true when considering statistics on a single granule. In this case, the number of observations is clearly fluctuating in time, changing according to the meteorological situations encountered by CloudSat along its orbit. We also note that the sample size is always quite small (below 200 samples), making the building of any statistics difficult when considering only a single granule.

When considering the tropics, from Fig. 2.6 it is obvious that below 10 km the number of observations is much smaller (about one third), mainly because of the reduced horizontal extension of the cloud structures at these

latitudes. On contrary, above 10 km, the presence of deep convection structures lead to a significant increase in number of observations. Also, differently from the mid-latitude cases, there is a reduction of cases from 6 km down to 2 km, likely due to the increase in occurrence of attenuation phenomena.

CloudSat	Mid-Latitudes South			Tropics		
$\Delta\bar{Z}_{CS} [mm^6m^{-3}]$	<i>Granule</i>	<i>12 hours</i>	<i>Day</i>	<i>Granule</i>	<i>12 hours</i>	<i>Day</i>
h=12 km	0.29	0.07	0.04	4.99	1.01	0.43
h=10 km	2.18	0.10	0.08	16.69	1.89	0.87
h=8 km	8.18	0.49	0.36	17.46	3.10	1.74
h=6 km	9.33	1.46	1.15	30.64	3.21	1.70
h=4 km	13.69	2.94	1.92	14.90	4.36	2.56
h=2 km	11.55	2.25	1.48	4.09	0.89	0.40

Table 2.1: Oscillation range of CloudSat reflectivity mean value at different time windows.

CloudSat	Mid-Latitudes South			Tropics		
$\Delta\sigma_{Z_{CS}} [mm^6m^{-3}]$	<i>Granule</i>	<i>12 hours</i>	<i>Day</i>	<i>Granule</i>	<i>12 hours</i>	<i>Day</i>
h=12 km	0.29	0.17	0.12	9.33	4.13	2.57
h=10 km	4.34	0.93	0.65	12.86	4.52	2.52
h=8 km	8.89	1.82	1.27	14.45	5.90	3.65
h=6 km	12.00	3.44	2.29	19.01	4.01	2.18
h=4 km	11.59	3.84	2.49	12.29	3.21	2.27
h=2 km	9.68	3.91	2.55	6.03	1.56	0.94

Table 2.2: Oscillation range of CloudSat reflectivity standard deviation evaluated at different time windows.

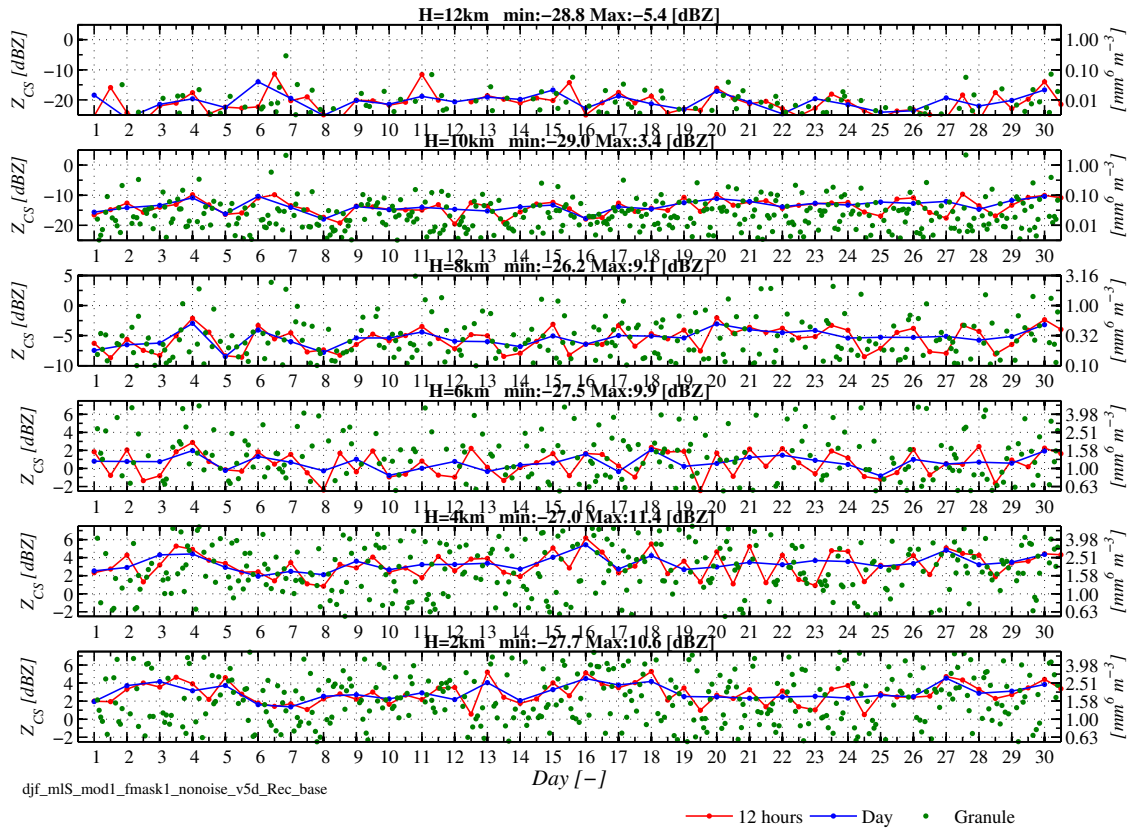


Figure 2.1: Time series of mean CloudSat reflectivity for the period from 1 to 30 January 2007, considering observations at mid-latitudes South (30°S-60°S). Each line refers to the time window stepping indicated in the legend. Different panels contain data at the altitude level (H) shown in the title.

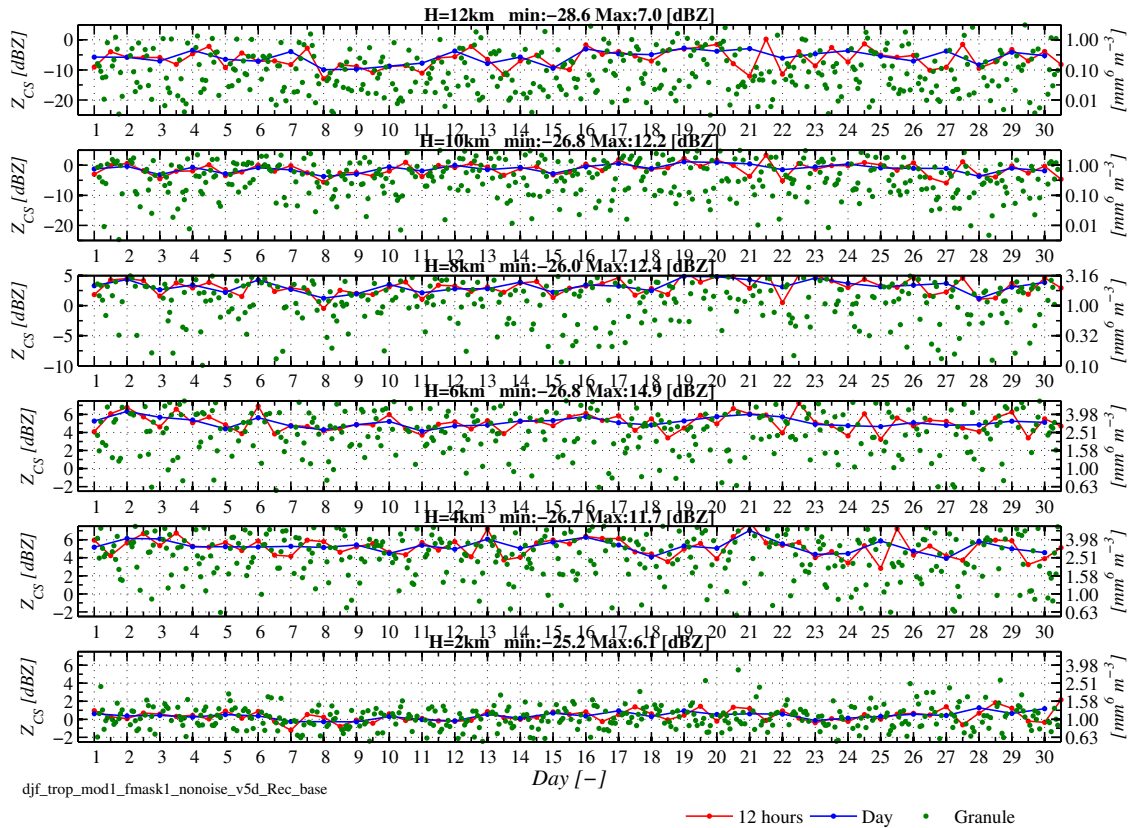


Figure 2.2: Same as Fig. 2.1, but considering observations in the tropics (30°S-30°N).

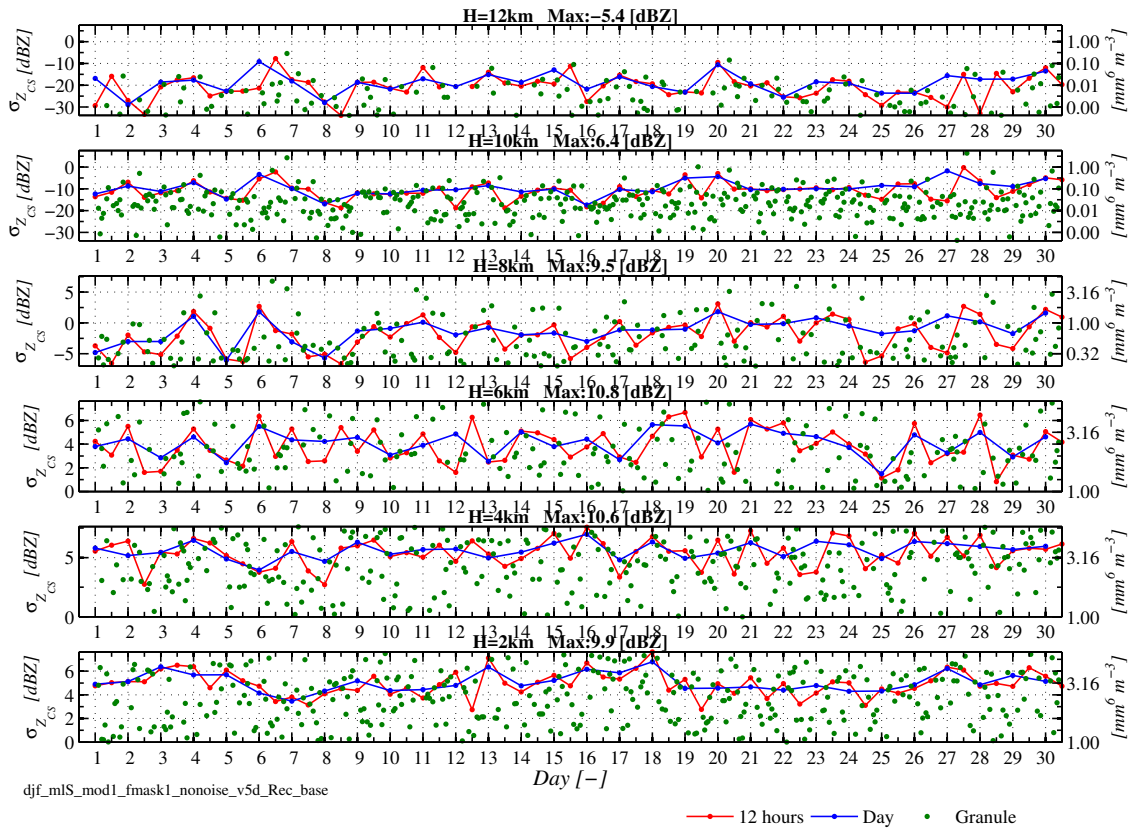


Figure 2.3: Same as Fig. 2.1, but for time series of CloudSat reflectivity standard deviation considering observations at mid-latitudes South (30°S-60°S).

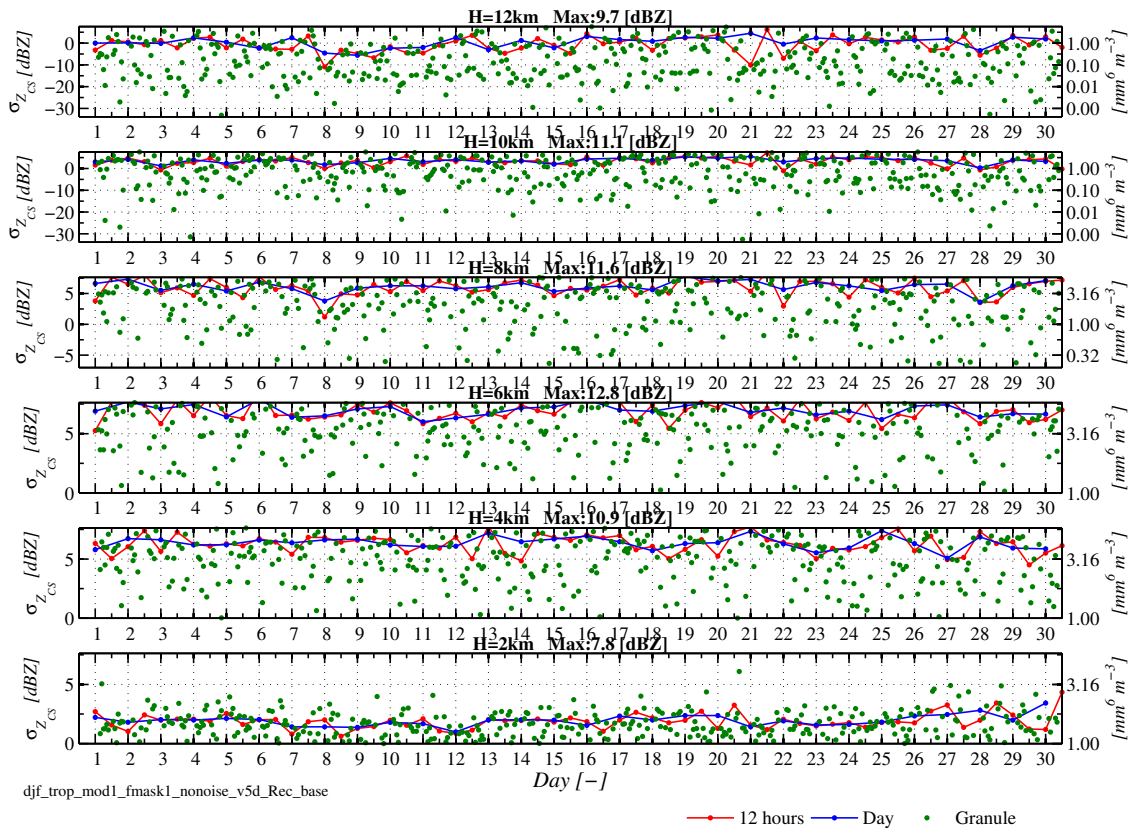


Figure 2.4: Same as Fig. 2.3, but considering observations in the tropics (30°S-30°N).

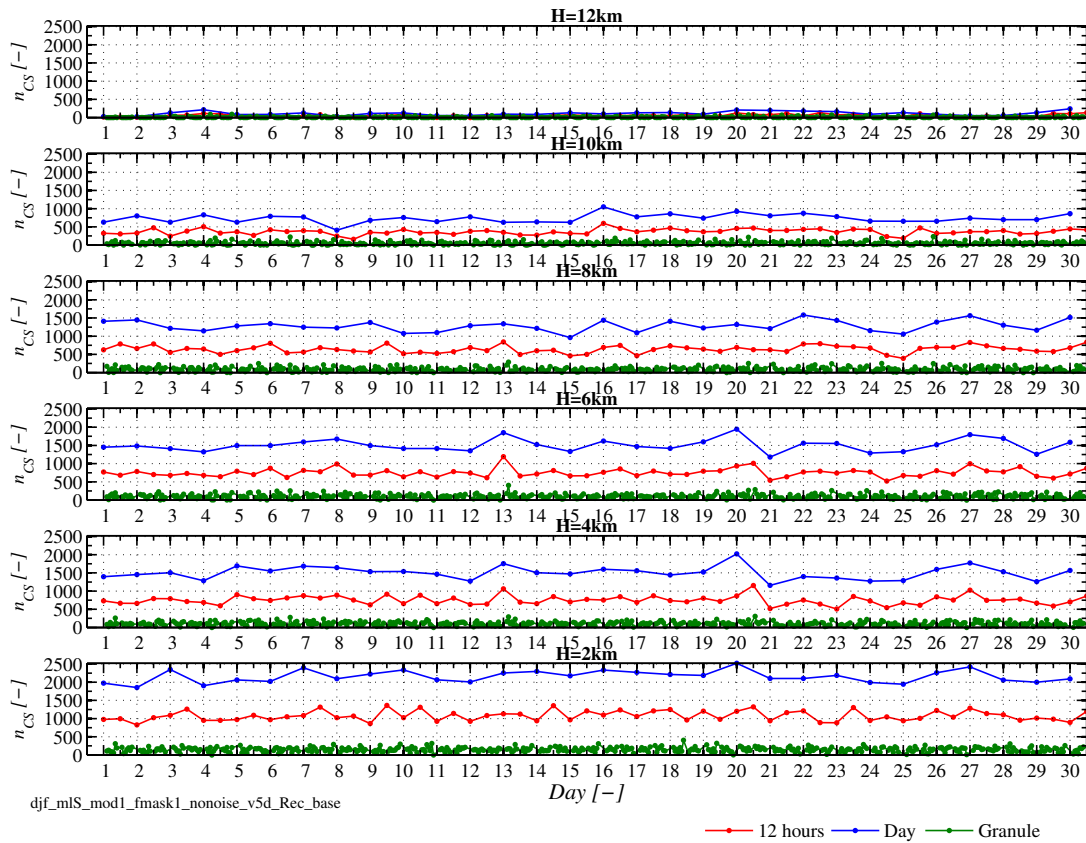


Figure 2.5: Same as Fig. 2.1, but for time series of CloudSat reflectivity sample number considering observations at mid-latitudes South (30°S-60°S).

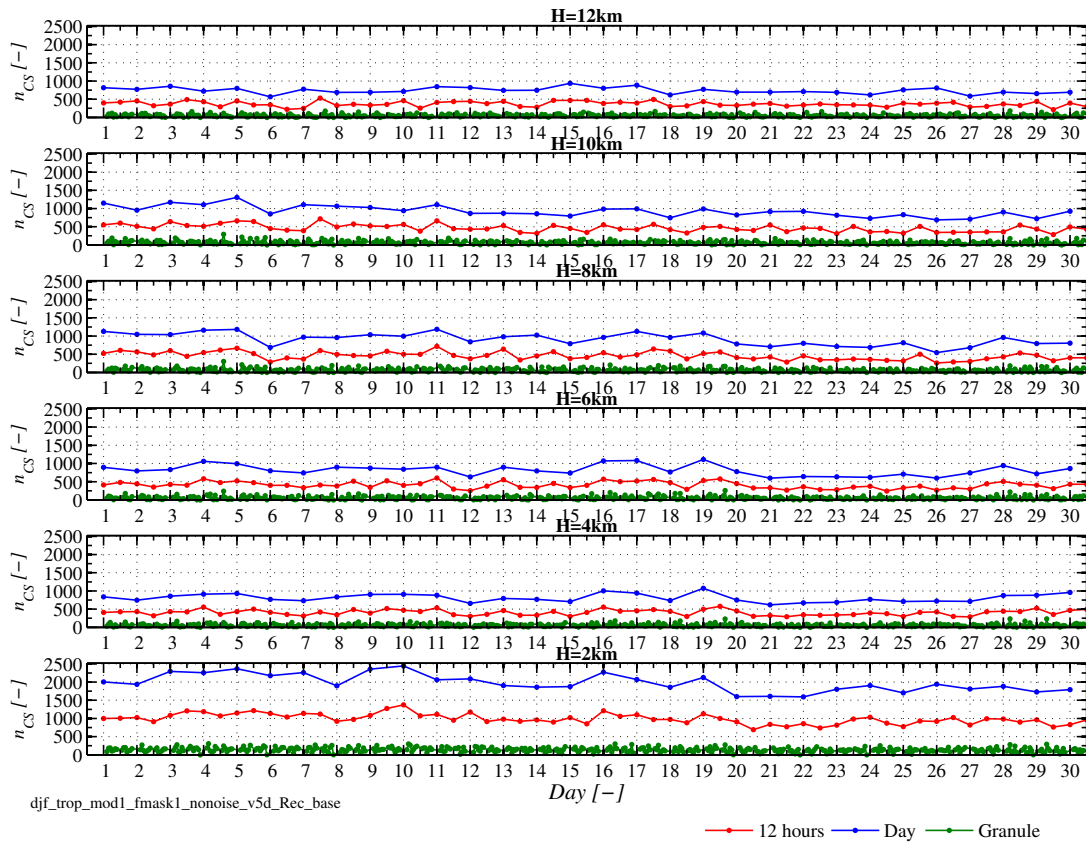


Figure 2.6: Same as Fig. 2.5, but considering observations in the tropics (30°S-30°N).

2.2 Time series of CloudSat reflectivity FG departures

Reflectivity FG departures (δZ) have been evaluated running the ZmVar radar operator with input profiles from the ECMWF short-range forecasts. These inputs have been used in 30-minute intervals, consistent with the ECMWF operational assimilation/monitoring system.

The basic assumption underlying the continuous monitoring of differences between observations and the corresponding quantity derived from short-term forecasts from a NWP model is that the latter is able to reproduce the observable with a satisfactory accuracy, consistently in time. The capability of the ECMWF forecast model (Integrated Forecast System, IFS) in representing clouds and simulated CloudSat observations has been previously documented by [Di Michele et al. \(2012\)](#). As an illustration, Fig. 2.7 shows CloudSat observations along a granule on 1 January 2007, together with the corresponding vertical curtain of radar reflectivity simulated using ZmVar on the IFS forecasts. Simulated observations are evaluated at model resolution by averaging the reflectivities of the hydrometeor-filled subcolumns in the grid box, considering only values above the minimum detectable signal. For consistency, CloudSat profiles have been horizontally averaged to match the coarser model resolution (about 25 km). Comparing the two panels, we note that the forecast model is able to realistically reproduce the cloud structures, capturing all main features. The general distribution and magnitude of radar reflectivity values are also well represented, although simulations show a coarser resolution despite CloudSat observations being averaged (horizontally and vertically) to the model grid resolution. Larger discrepancies occur in the tropical regions, recognizable by the higher freezing level (black dashed line). These cloud regimes are the most difficult to represent, given their small scale and short temporal duration that can lead to errors in intensity and/or location. Note that the CloudSat data are missing in the lowest kilometre due to the removal of the data bins contaminated by surface clutter.

Our aim is to understand if the forecast skill can result in an advantage of the FG departures over the observations alone in monitoring the quality of the data.

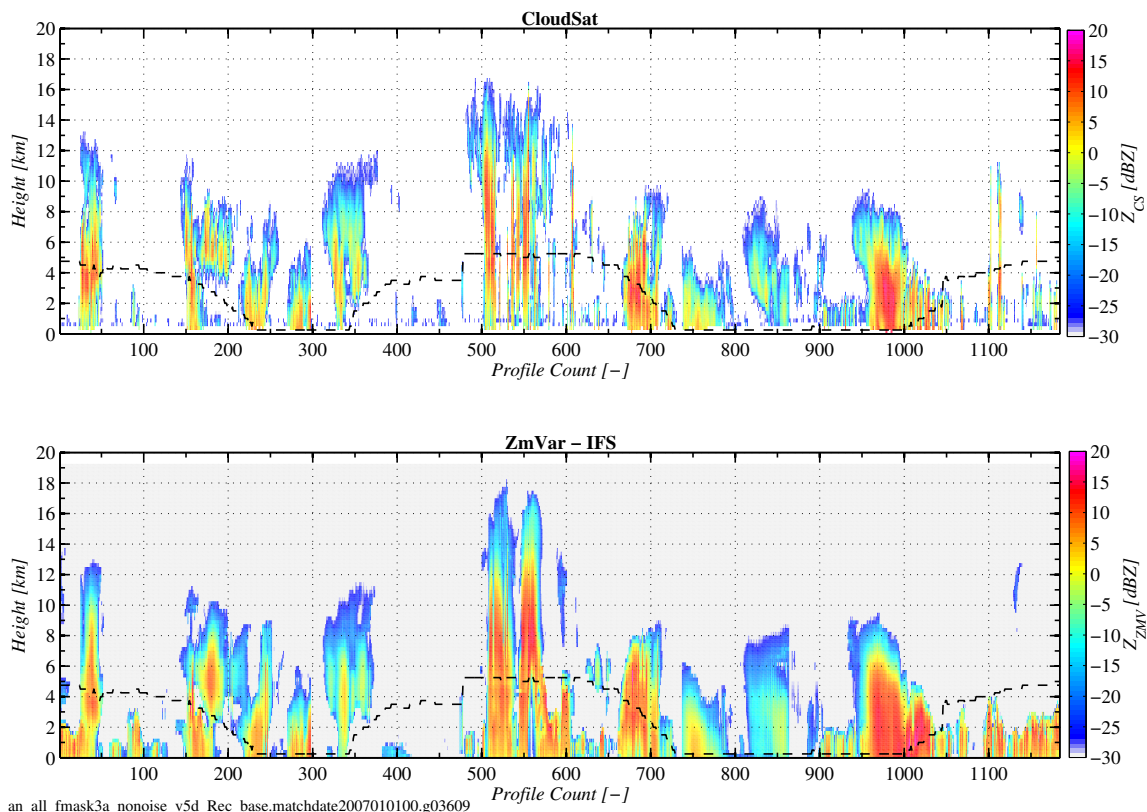


Figure 2.7: Top panel: CloudSat observations (averaged to model resolution) along granule 3609 on 1st January 2007. Bottom panel: the corresponding simulated reflectivities using ZmVar on the ECMWF model short-term forecasts.

In WP-1100 (Di Michele et al., 2014), a quality control procedure to be used prior to data assimilation was developed in order to ingest only observations for which the corresponding FGs were close enough. Essentially, the screening technique retains only those observations for which the corresponding FGs were smaller than a chosen maximum value. However, this type of screening is not appropriate when interested in the monitoring for the check of data quality. In fact, cases corresponding to measurement issues could be filtered out if leading to large departures, therefore not appearing into the FG departures statistics used for monitoring. Then, for data quality monitoring, a different method has been devised which is not based on the checking of FG departures, but instead considers less strict criteria, independently for simulations and observations. As shown in Fig. 2.8, the selected interval ranges where FG reflectivity must lie in order to be used for monitoring differ with altitude. The limits have been chosen based on the scatterplots shown in WP-1100 report (Fig. 4.1 and Fig. 4.2 of Section 4 in Di Michele et al., 2014), aiming at selecting only the ranges where there is the best correlation between observations and simulations. An important secondary effect of this screening is the reduction in the range of variability of the monitoring quantity. The range of reflectivity which naturally extends over 5 orders of magnitude is reduced to three, leading to a better resilience of statistics to outliers.

The number of observations passing the screening also constitutes an important piece of information for monitoring. It complements the departures since a drop in their number would indicate a decrease in agreement (because of less cases passing through the screening).

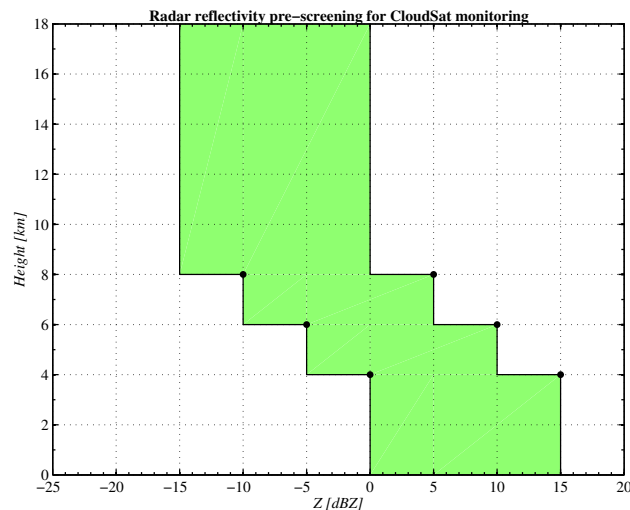


Figure 2.8: Schematic view of the screening performed prior to monitoring. Green shaded areas indicate the reflectivity range in which FGs are accepted across altitudes.

Figure 2.9 shows, with the figure layout used before in Section 2.1, the number of samples $n_{\delta Z}$ at Southern mid-latitudes passed through quality control of δZ . Comparing with Fig. 2.5, we note that up to 25 % of the data are removed and that the heavier screening occurs at altitudes where liquid precipitation is present. This is a consequence of the well known difficulty of the model in partitioning the relative amount of cloud liquid and (light) liquid precipitation. In fact, since the radar signal from non-precipitating liquid is considerably weaker than the one of rain, large discrepancies between model and observations can arise, leading in turn to a large number of rejections. In Fig. 2.10 similar plots are given for observations at tropical latitudes over the same period. In this case, the screening of data can reach 50 % below 6 km, reflecting again the larger discrepancies between simulations and observations under the meteorological conditions typical of these latitudes.

The time series of mean FG departures relative to observations at mid-latitudes South and tropics, are shown in Fig. 2.11 and Fig. 2.12. Similarly as for CloudSat observations, for the mean FG departures $\overline{\delta Z}$ we can also consider the difference between the maximum and minimum values along the monitoring period, $\Delta \overline{\delta Z}$. Table 2.3 reports the values at the reference altitude heights, separately for the Southern mid-latitudes and the tropics.

Comparing the values of $\Delta\bar{\delta Z}$ with the ones of $\Delta\bar{Z}_{CS}$ in Table 2.1, we note that the range of variation of FG departures is lower than the one of the observations alone by a factor of 3 or more at all altitudes.

As for observations, it is worth considering the standard deviation $\sigma_{\delta Z}$ of FG departures. The $\sigma_{\delta Z}$ time series are shown in Fig. 2.13 and Fig. 2.14, for Southern mid-latitudes and tropics, respectively. An oscillation range $\Delta\sigma_{\delta Z}$ can be also defined for departures, as the maximum of $\sigma_{\delta Z}$ along the monitoring period. Table 2.4 gives the values of $\sigma_{\delta Z}$ corresponding to Fig. 2.13 and Fig. 2.14. Comparing with Table 2.2, it is clear that monitoring FG departures instead of observations alone gives a reduction in the values of the standard deviation. This result, together with the similar conclusion for the mean time series, suggests that the monitoring of CloudSat FG departures should be preferable over the one of observations-only since it would allow the identification of anomalies of smaller values.

In all previous plots (for both observations and FG departures) it was evident that, when statistics are computed on a single granule (i.e. orbit), time series of mean and standard deviation are changing very rapidly. The main reason for this must be found in the narrow swath of CloudSat, leading to the observation of relatively few cloud structures in one granule, and that those structures are very likely the same in the consequent orbit. This is also reflected in the small (and also rapidly changing) number of observations falling in one granule (less than 100 *per* level). In spite of this, continuously comparing CloudSat observations against the similar quantity simulated through a forecast model can be useful also at time scales of a single orbit. This is possible through the monitoring of the correlation between the granule-mean CloudSat and FG reflectivities as demonstrated in Fig. 2.15 and Fig. 2.16 displaying the temporal evolution of these correlations. Noticeably, in the Southern mid-latitudes (Fig. 2.15) it gets consistently between 0.7 and 1 at altitudes between 4 and 8 km. The agreement is worse in the tropics (Fig. 2.16). Especially when considering shorter time lengths, the correlation can drop to values below 0.5 for periods of several days. This degradation can be attributed to intense, relatively scattered cloud structures typical at the tropics. Under these conditions, it is difficult for the model to match location and horizontal extension of the observed structures.

CloudSat - IFS	Mid-Latitudes South			Tropics		
	Granule	12 hours	Day	Granule	12 hours	Day
$\Delta\bar{\delta Z} [mm^6 m^{-3}]$						
h=12 km	0.48	0.37	0.37	0.20	0.06	0.03
h=10 km	1.01	0.45	0.33	0.70	0.10	0.06
h=8 km	2.35	0.49	0.32	1.00	0.17	0.07
h=6 km	14.32	1.42	1.03	1.00	0.20	0.13
h=4 km	23.67	3.83	1.95	1.50	0.22	0.15
h=2 km	22.39	5.56	3.40	0.50	0.16	0.12

Table 2.3: Oscillation range of the CloudSat reflectivity mean FG departures evaluated at different time windows.

CloudSat - IFS	Mid-Latitudes South			Tropics		
	Granule	12 hours	Day	Granule	12 hours	Day
$\sigma_{\delta Z} [mm^6 m^{-3}]$						
h=12 km	0.32	0.34	0.34	0.25	0.07	0.04
h=10 km	0.43	0.31	0.30	0.31	0.05	0.04
h=8 km	1.25	0.76	0.77	0.41	0.14	0.09
h=6 km	5.20	2.27	2.23	0.55	0.08	0.03
h=4 km	12.52	7.23	5.92	0.68	0.12	0.06
h=2 km	12.65	8.40	7.63	0.52	0.10	0.06

Table 2.4: Standard deviation of CloudSat reflectivity FG departures evaluated at different time windows.

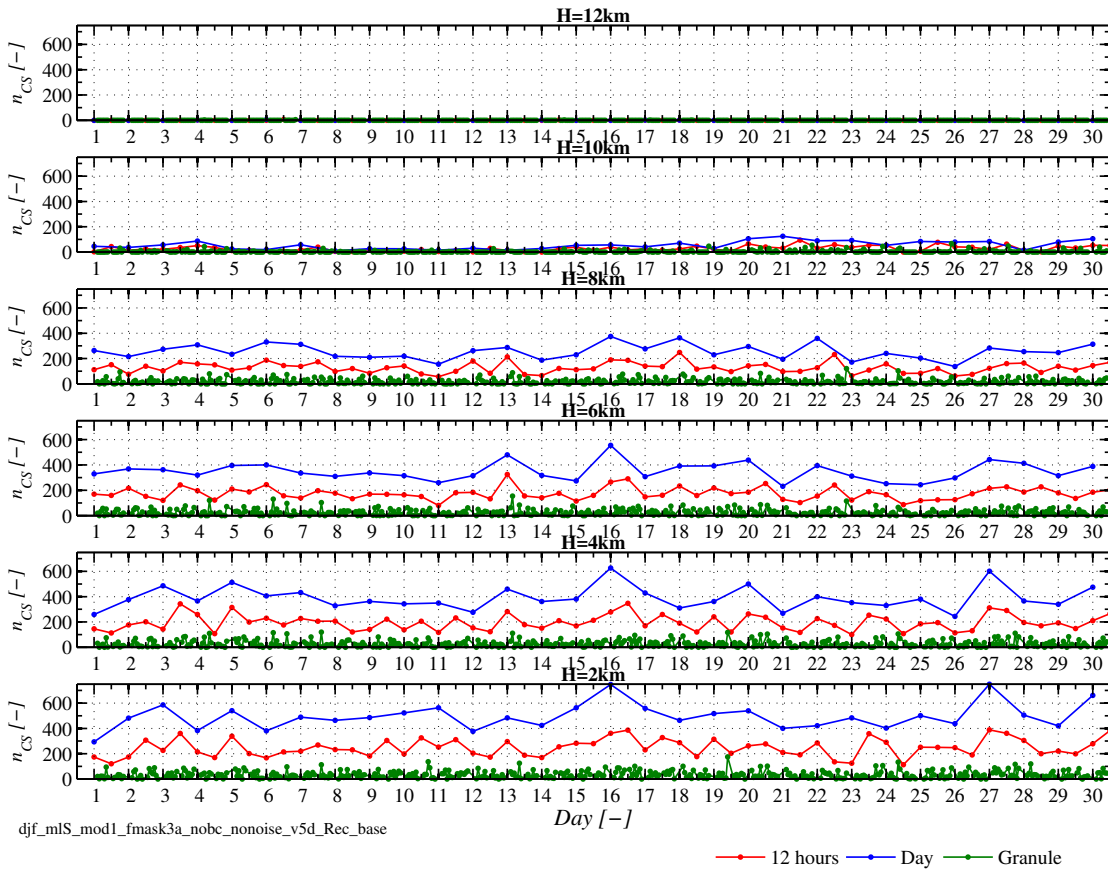


Figure 2.9: Same as Fig. 2.5, but after quality control.

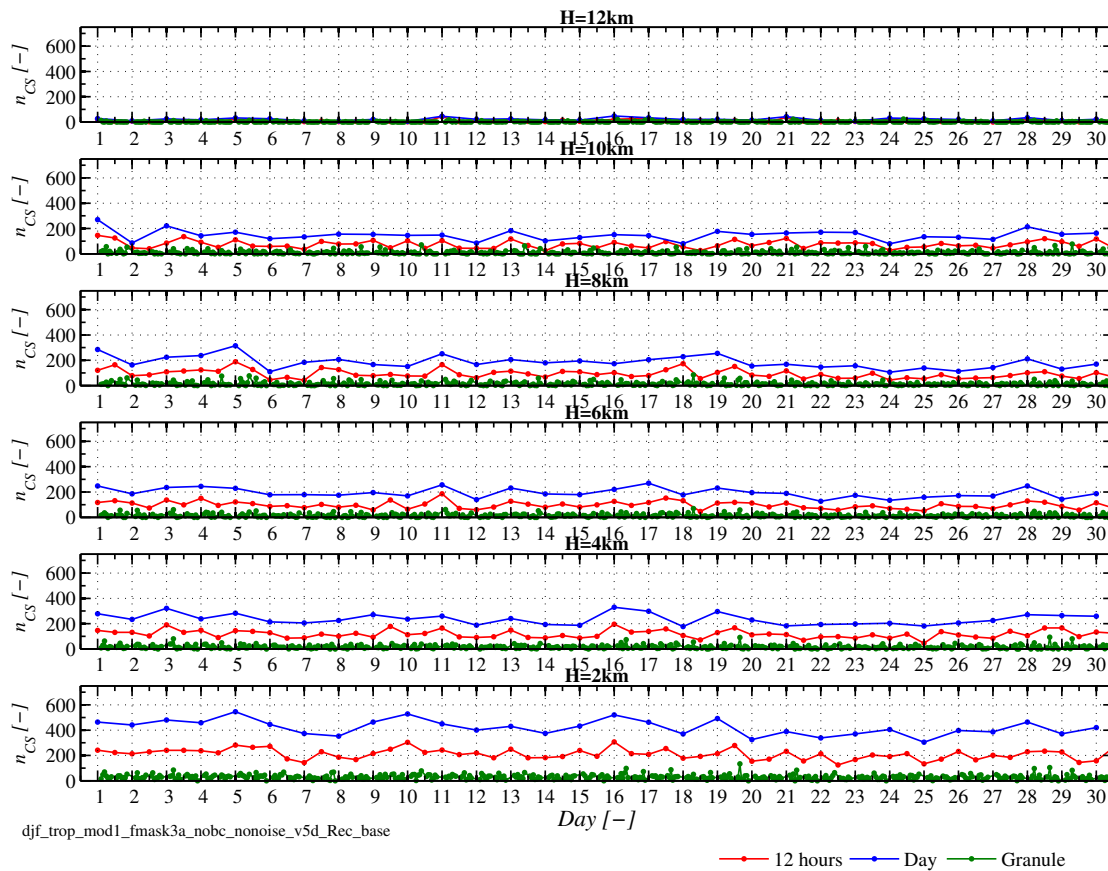


Figure 2.10: Same as Fig. 2.9, but considering observations in the tropics (30°S-30°N).

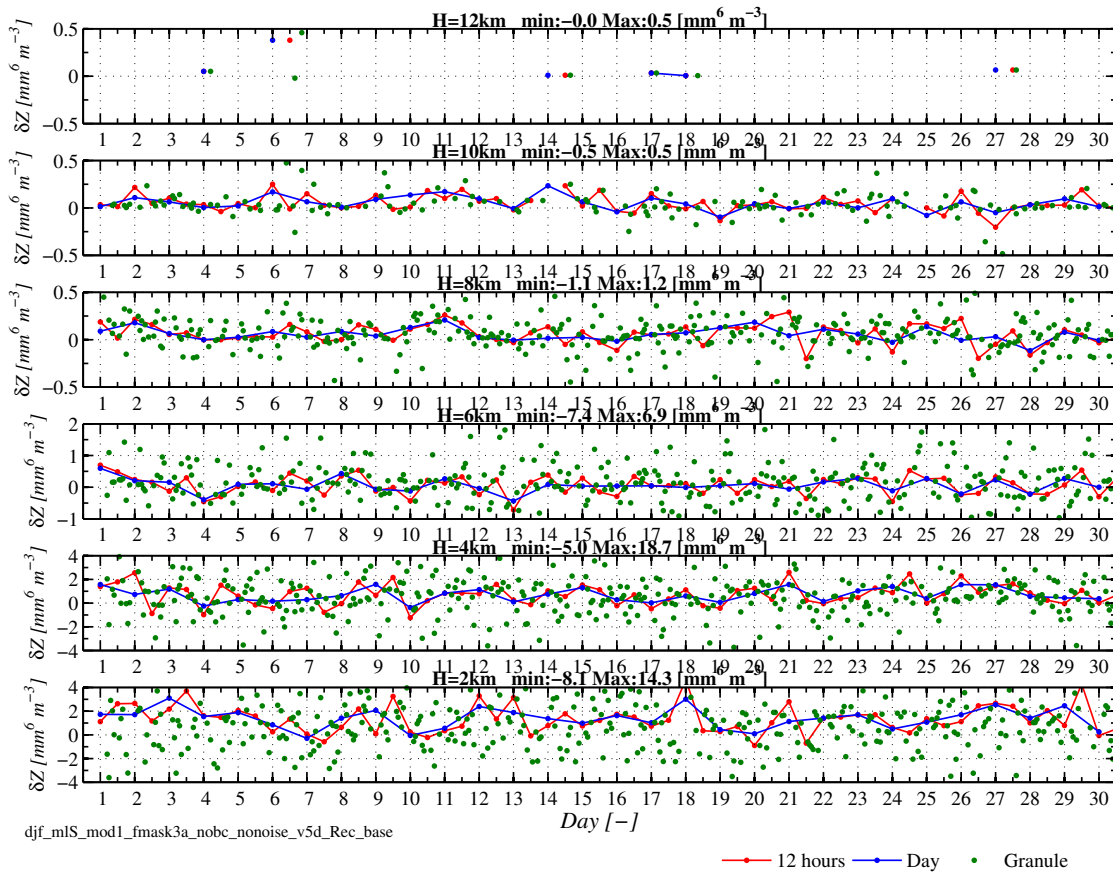


Figure 2.11: Same as Fig. 2.1, but for time series of mean CloudSat reflectivity first-guess departures considering observations at mid-latitudes South (30°S-60°S).

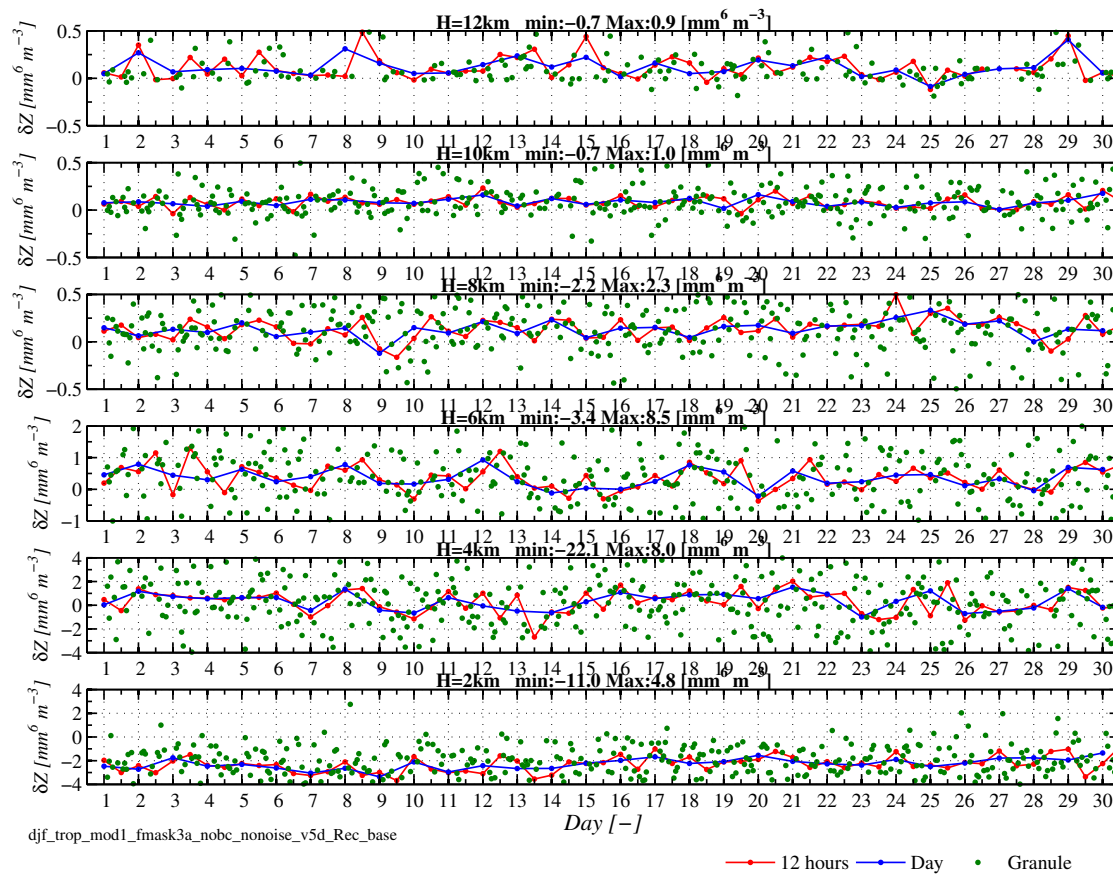


Figure 2.12: Same as Fig. 2.11, but considering observations in the tropics (30°S-30°N).

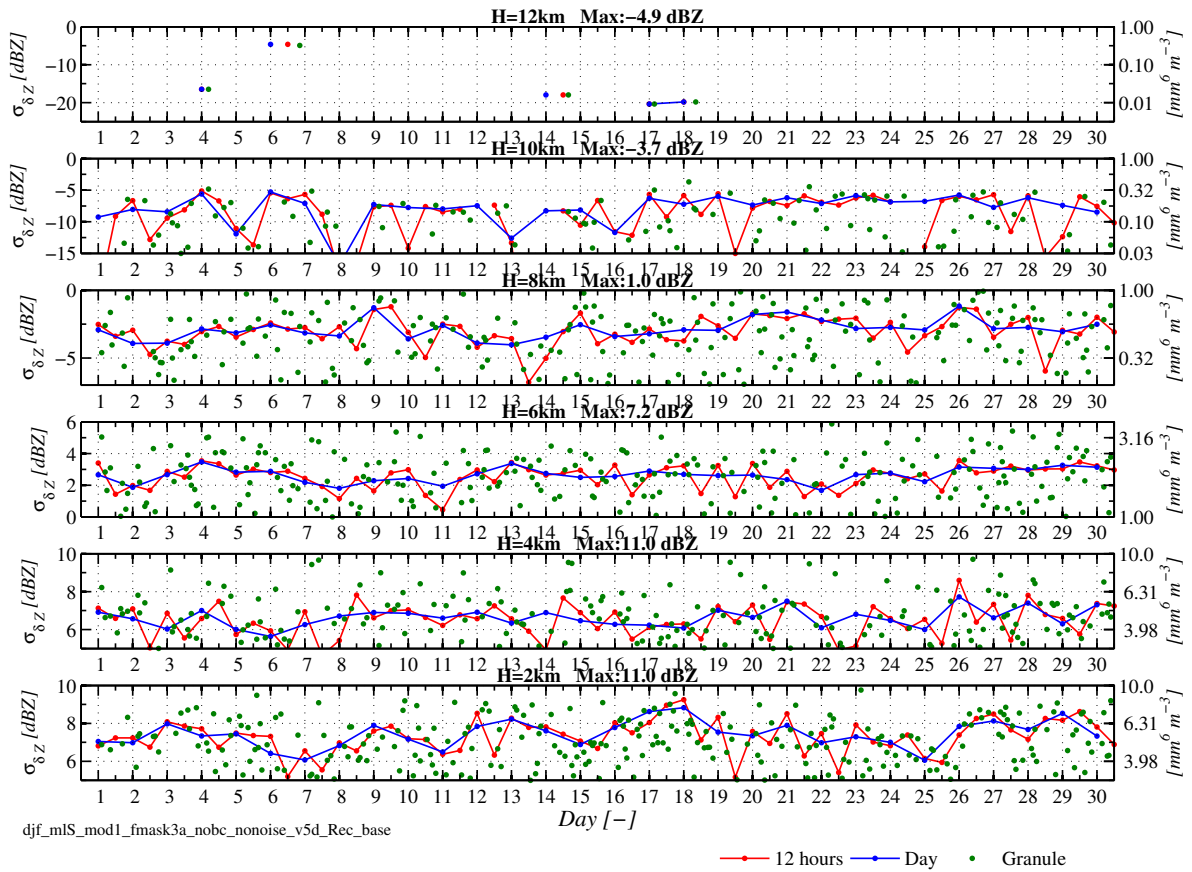


Figure 2.13: Same as Fig. 2.1, but for time series of CloudSat reflectivity first-guess departure standard deviation, considering observations at mid-latitudes South (30°S-60°S).

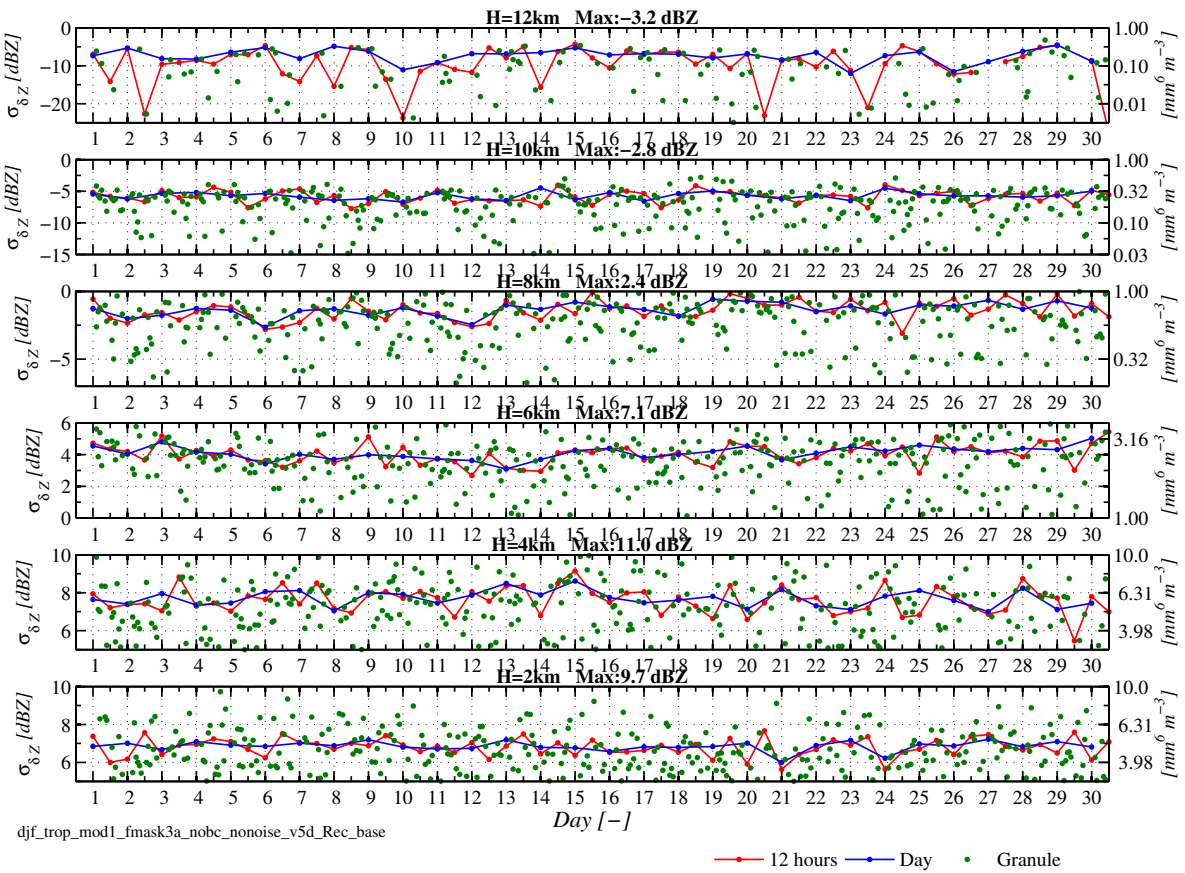


Figure 2.14: Same as Fig. 2.13, but considering observations in the tropics (30°S-30°N).

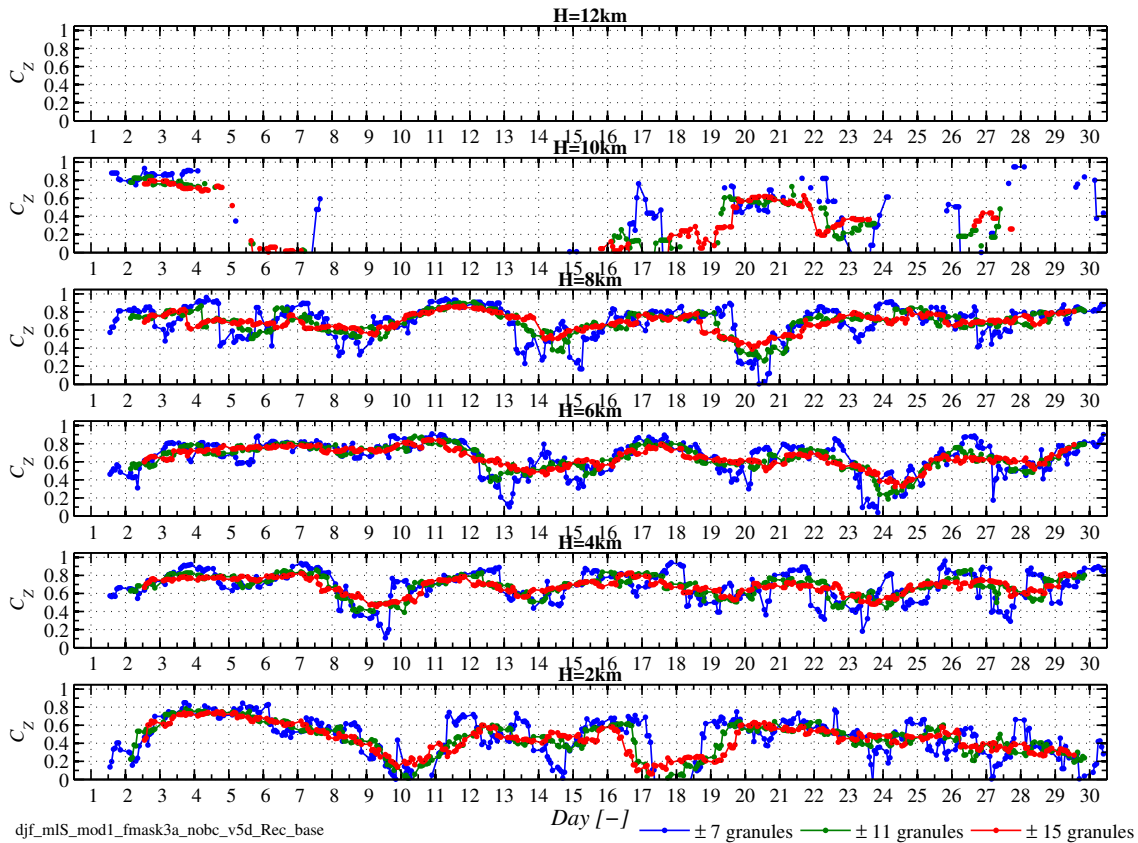


Figure 2.15: Time series of correlation between granule-mean CloudSat reflectivity and IFS-ZmVar reflectivity for the period of 1-30 January 2007, considering observations at mid-lat. South (30°S-60°S). Each line refers to the time length indicated in the legend. Different panels contains data at the altitude level (H) shown in the title.

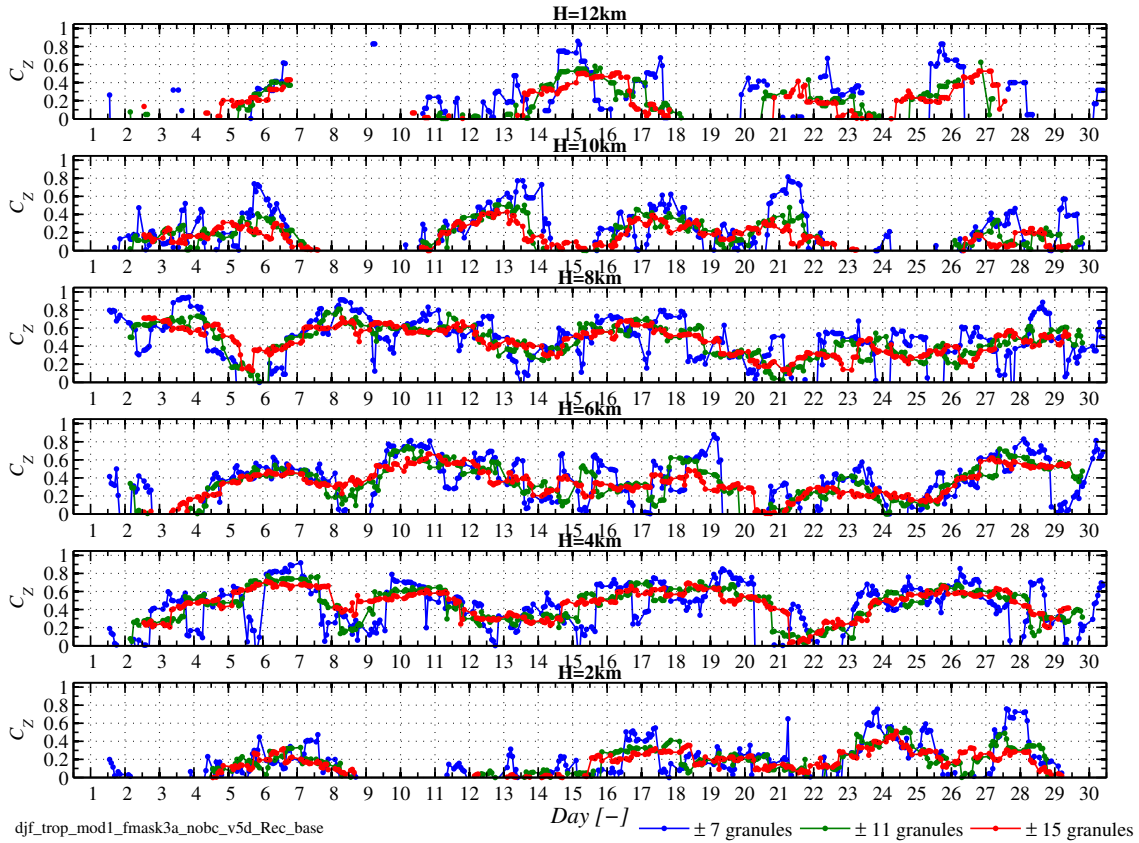


Figure 2.16: Same as Fig. 2.15, but considering observations in the tropics (30°S-30°N).

3 Monitoring of cloud-top height

Another quantity considered for the monitoring is cloud-top height (CTH) derived from CloudSat reflectivity measurements. The height of cloud-top from CloudSat observations (h_{CS}^{top}) can be defined as the altitude of the most high radar bin with reflectivity exceeding the minimum detectable value Z_{CS}^{min} , i.e:

$$Z_{CS}(h) < Z_{CS}^{min} \quad \forall h > h_{CS}^{top} \quad (3.1)$$

where Z_{CS}^{min} has been set equal to -29 dBZ, accordingly to the CloudSat radar specifications. In principle, CTH monitoring has a number of advantages over the reflectivity monitoring:

1. Using one piece of information from each vertical profile of measurements makes the process of monitoring simpler than considering the full reflectivity profile;
2. CTH is very sensitive to the instrument performance;
3. The same approach can be easily applied to lidar observations, providing the simultaneous monitoring of the instruments in a consistent way, with the possibility of cross checks.

Similarly to the monitoring of reflectivity in Section 2, in Subsection 3.1 the monitoring of Cloudsat cloud-top height alone will be first investigated. In Subsection 3.2, FG departures will be taken into account deriving the model CTH counterpart to CloudSat using the IFS forecasts and the ZmVar radar forward operator.

3.1 Time series of cloud-top height from CloudSat

The monitoring of h_{CS}^{top} has been performed following the same approach used for reflectivities. Therefore, the temporal evolution of CTH statistics (mean, standard deviation, number of samples) has been evaluated using CloudSat data for the same period of January 2007, distinguishing among the same geographical regions. Time series of mean CTH, \bar{h}_{CS}^{top} are shown in Fig. 3.1, where the top panel considers observations at Southern mid-latitudes and the bottom refers to tropical cases. In both regions we note that only the 24-hour averaging is able to reduce the rapid oscillations of the mean to values below one kilometre. Interestingly, the mean values at the tropics for 12- and 24-hour periods are comparable or slightly lower than that at mid-latitudes. The reason for this relates to the shallow convective clouds, which being only less than few kilometres high, contribute to decrease the average. The corresponding temporal evolution of standard deviation $\sigma_{h_{CS}^{top}}$ is shown in Fig. 3.2. As for the mean, the granule and 12-hour curves evolve in time with strong oscillations. Comparing mid-latitudes with tropics, we have the expected result of the latter being overall larger (of about one kilometre). Again as done for reflectivities, we can define an oscillation range $\Delta\bar{h}_{CS}^{top}$ of the mean CTH, defined as the difference between maximum and minimum values in the monitoring period. In a similar manner, the range of variation $\Delta\sigma_{h_{CS}^{top}}$ of the standard deviation can be introduced. Table 3.1 contains the values of $\Delta\bar{h}_{CS}^{top}$ and $\Delta\sigma_{h_{CS}^{top}}$ for January 2007, corresponding to Fig. 3.1 and 3.2.

CloudSat	Mid-Latitudes South			Tropics		
	Granule	12 hours	Day	Granule	12 hours	Day
-						
$\Delta\bar{h}_{CS}^{top} [km]$	7.84	1.70	1.21	10.10	1.61	1.30
$\Delta\sigma_{h_{CS}^{top}} [km]$	5.18	0.80	0.50	6.31	0.90	0.41

Table 3.1: Oscillation range of mean and standard deviation CloudSat-derived CTH evaluated at different time windows.

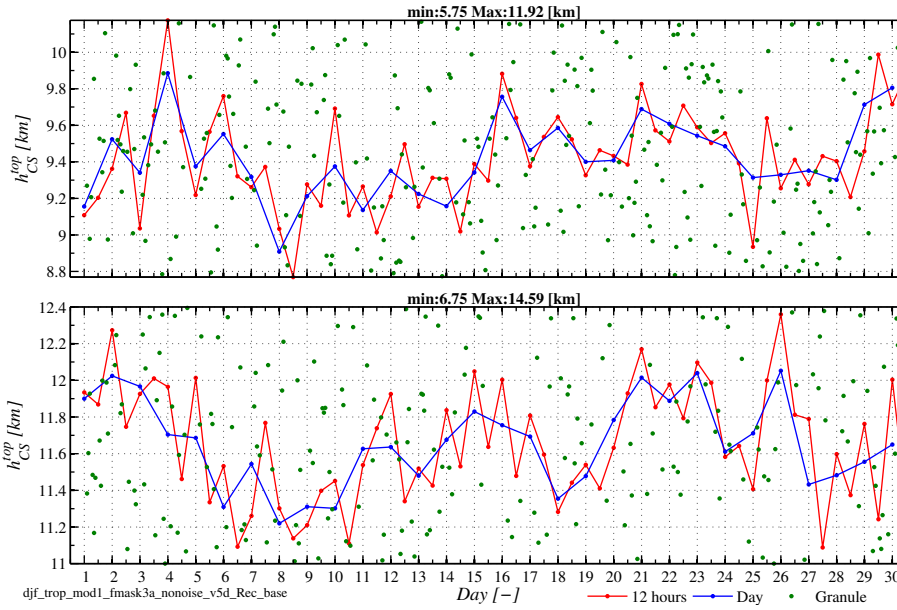


Figure 3.1: Time series of mean CloudSat-derived CTH for the period from 1 to 30 January 2007. Each line refers to the time window stepping indicated in the legend. Top panel is for observations at mid-latitudes South (30°S-60°S), and bottom panel uses observations in the tropics (30°S-30°N).

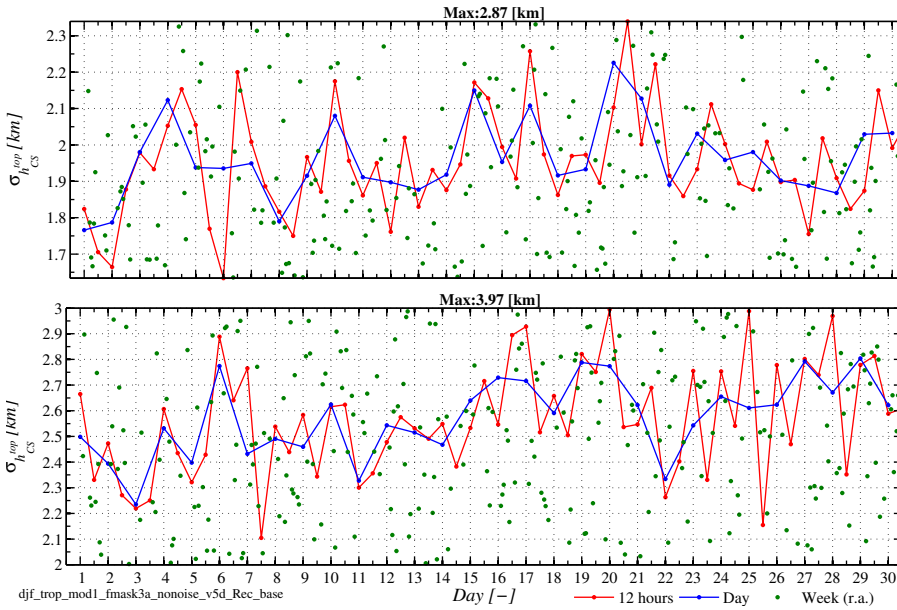


Figure 3.2: Same as 3.1, but for time series of standard deviation of CloudSat-derived CTH.

3.2 Time series of cloud-top height departures

In order to evaluate the CTH departures δh^{top} , the model equivalent to CloudSat radar reflectivity has been simulated using ZmVar. Similarly to Eq. 3.1, CTHs from simulated reflectivities h_{ZMV}^{top} have been defined as the values of h for which:

$$Z_{ZMV}(h) < Z_{CS}^{min} \quad \forall h > h_{ZMV}^{top} \quad (3.2)$$

Figure 3.3 gives the CTH corresponding to reflectivities shown in Fig. 2.7. Although only in a qualitative way, the plot shows a good correlation between the CTH resulting from CloudSat observations and the one derived from ZmVar reflectivities based on the IFS forecasts.

As done for the monitoring of reflectivities, we want to investigate if there are any advantages in considering FG departures compared to using CloudSat CTH alone. Therefore, prior to the use of departures, a necessary step is the assessment of the quality of the agreement between FG and observations. This is particularly important when aim of the monitoring is the detection of instrument problems: the better the correlation between FG and observations, the smaller the anomaly that in principle can be identified.

Figures 3.4 and 3.5 show, for mid-latitudes and tropics respectively, the scatterplot between the CTH from CloudSat and the one from the IFS forecasts. In both scatterplots two distinct clusters of points can be seen along the diagonal: a first one at altitudes below 5 km (low clouds) and a second one above 5 km (high clouds). Although different in number of occurrence, two clusters along the axes represent those situations where observations and the model have the largest disagreement. Looking at Fig. 3.3 and Fig. 2.7, one can notice that this is usually caused by a misplacement between observed and simulated clouds.

Similarly to what was done for the reflectivity monitoring, a screening procedure is performed prior to the actual monitoring of CTH FG departures. Based on Fig. 3.4 and Fig. 3.5, two regions of high correlation can be isolated selecting only cases where CloudSat CTH and IFS CTH (FG) are below 5 km or both are above 5 km. These conditions are sufficient to keep out those situations where low clouds and high clouds are erroneously positioned. The detection of bias through CTH departures monitoring has been performed considering independently the two screening conditions (clouds below 5 km and clouds above 5 km). In this report, only the monitoring of high clouds will be reported since it is the one that gives the best results, and therefore better representing the CTH monitoring possibilities.

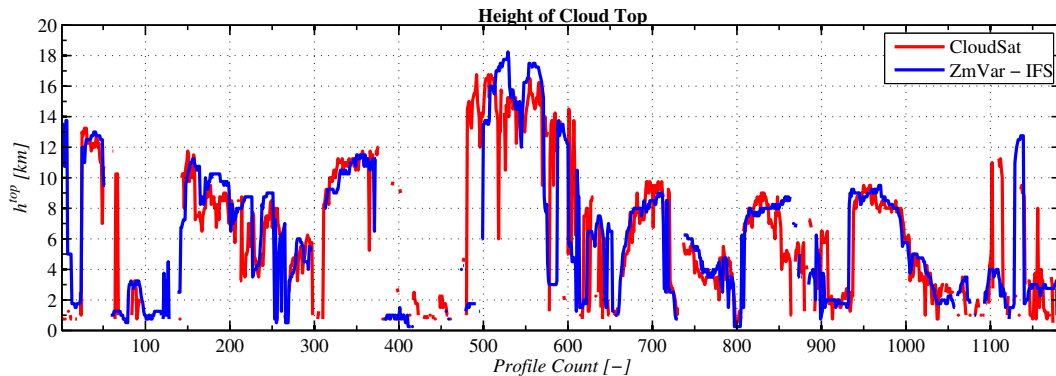


Figure 3.3: Height of cloud-top derived from CloudSat observations (red line) and from ZmVar reflectivities (blue line) corresponding to the data shown in Fig. 2.7.

Mean $\overline{\delta h^{top}}$, and standard deviation $\sigma_{\delta h^{top}}$ of CTH FG departures are shown in Fig. 3.6 and Fig. 3.7, respectively. The range of variation of the mean CTH departure $\Delta\overline{\delta h^{top}}$ and the maximum standard deviation $\Delta\sigma_{\delta h^{top}}$ are given in Table 3.2. Similarly as for the reflectivity monitoring, the range of variation of FG departures is more than twice lower than the one of CTH alone (See Table 3.1 for comparison).

CloudSat - IFS	Mid-Latitudes South			Tropics		
	Granule	12 hours	Day	Granule	12 hours	Day
$\overline{\delta h^{top}}$ [km]	2.56	0.51	0.35	4.74	0.45	0.25
$\sigma_{\delta h^{top}}$ [km]	2.09	0.40	0.20	2.26	0.30	0.15

Table 3.2: Mean oscillation range and standard deviation of CloudSat-derived CTH FG departures evaluated at different time windows.

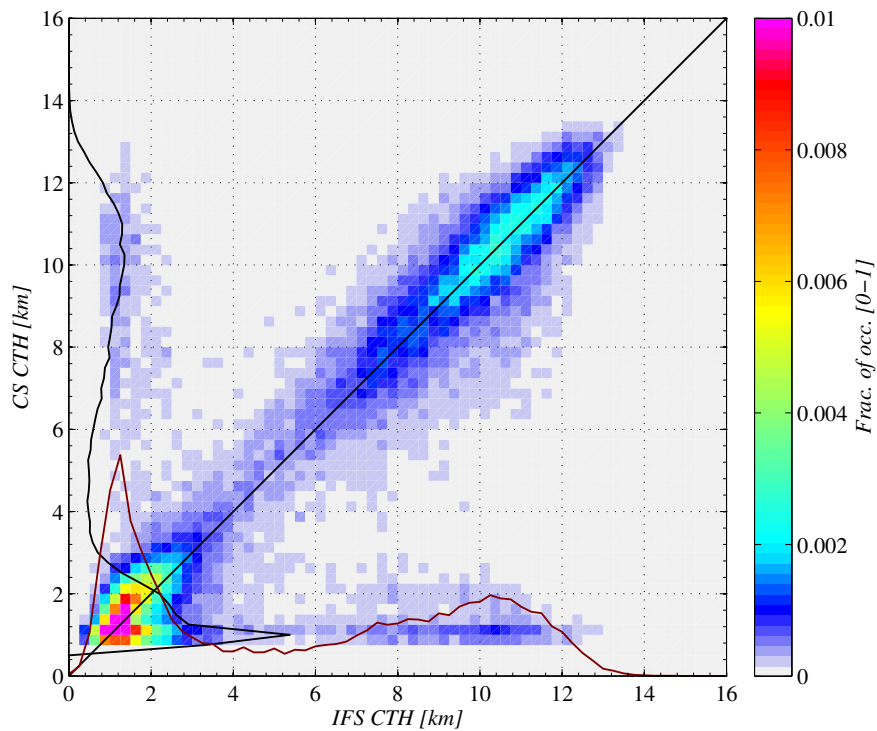


Figure 3.4: Scatter plot between cloud-top height derived from ZmVar reflectivity run using the IFS model data as input (on abscissa) and the one derived from CloudSat reflectivity (on ordinate) using observations over ocean matched with model data between 30°S and 60°S for the period of January 2007. Curves along axes show the relative occurrence of cloud-top height.

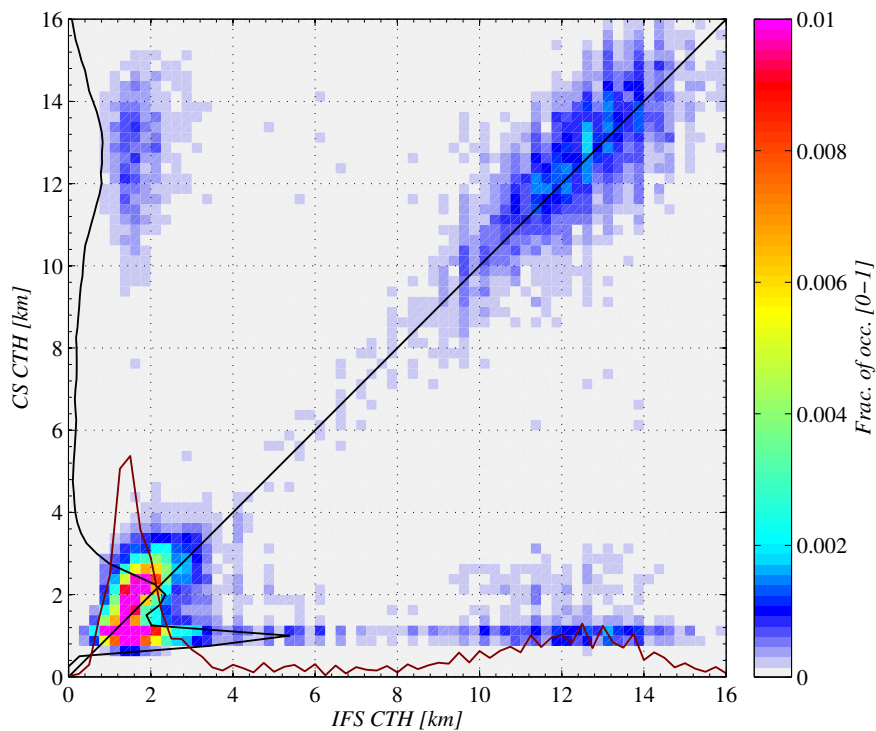


Figure 3.5: Same as 3.4, but considering observations in the tropics (30°S - 30°N).

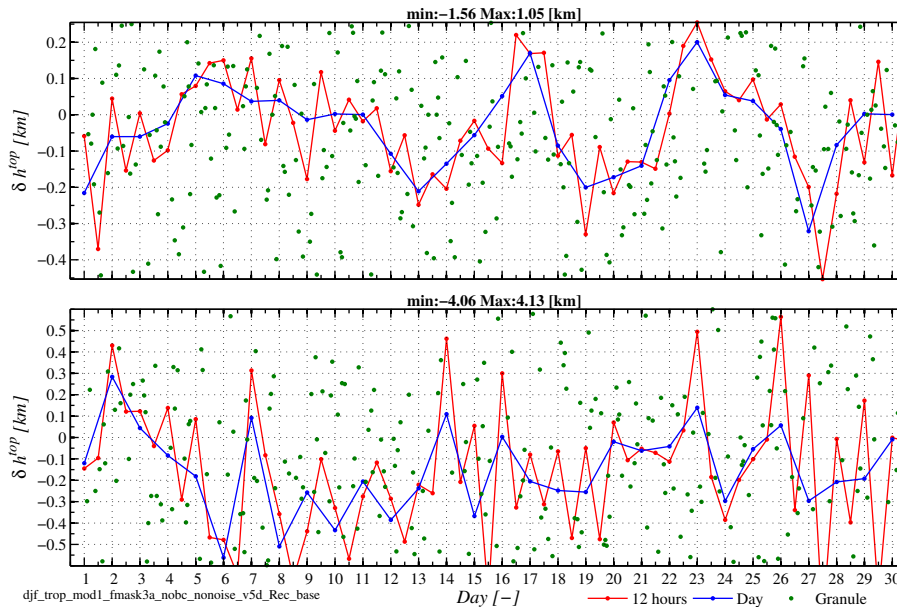


Figure 3.6: Same as 3.1, but for time series of CTH mean difference between CloudSat and IFS-ZmVar equivalents.

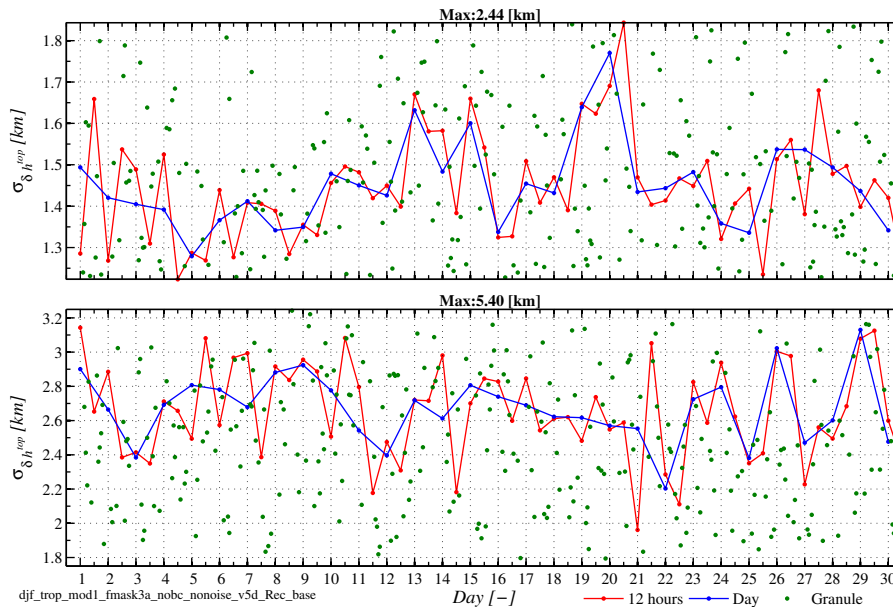


Figure 3.7: Same as 3.1, but for time series of standard deviation of CTH difference between CloudSat and IFS-ZmVar equivalents.

Fig. 3.8 shows the correlation between granule-mean CloudSat derived CTH ($\overline{h_{CS}^{top}}$) and IFS-ZmVar derived CTH ($\overline{h_{ZMV}^{top}}$). Oscillation of the correlation between granule means are reduced by increasing number of granules used for averaging. At mid-latitudes, this correlation is consistently between 0.8 and 1 for larger number of used granules. There is more variation in the tropics due to more scattered cloud structures, although there can be periods of several days with the correlation above 0.7.

Finally, Figure 3.9 shows the time series for the number of CloudSat-derived CTH (h_{CS}^{top}) samples, $n_{h^{top}}$. The variations are most evident at granule level and they are getting significantly reduced already for 12-hour averaging time window. Interestingly, time-averaged numbers are quite consistent for both tropics and mid-latitudes South.

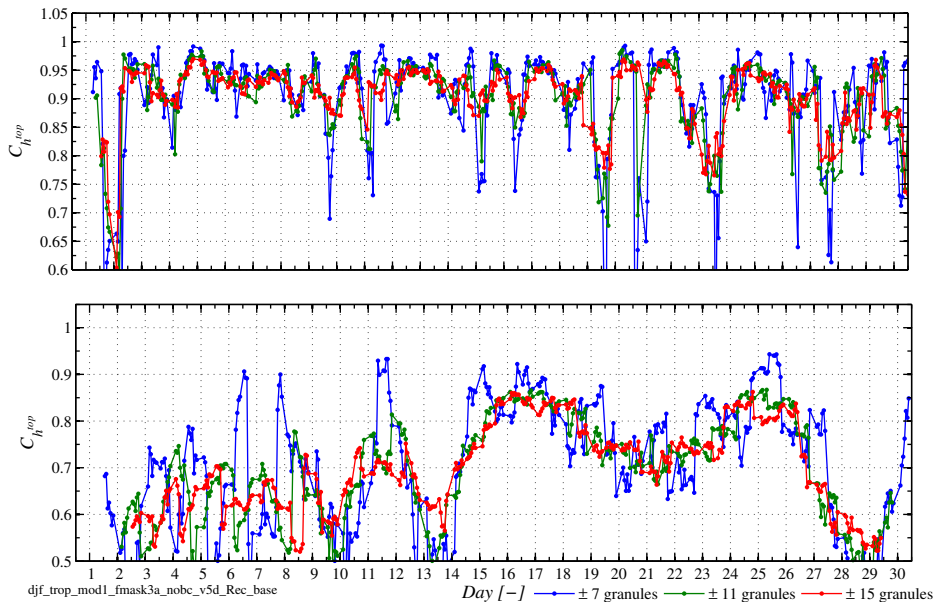


Figure 3.8: Time series of correlation between granule-mean CloudSat-derived and IFS-ZmVar derived CTH for the period from 1 to 30 January 2007. Each line refers to the time length used to evaluate the correlation as indicated in the legend. Top panel is for observations at mid-latitudes South (30°S-60°S), and bottom panel uses observations in the tropics (30°S-30°N).

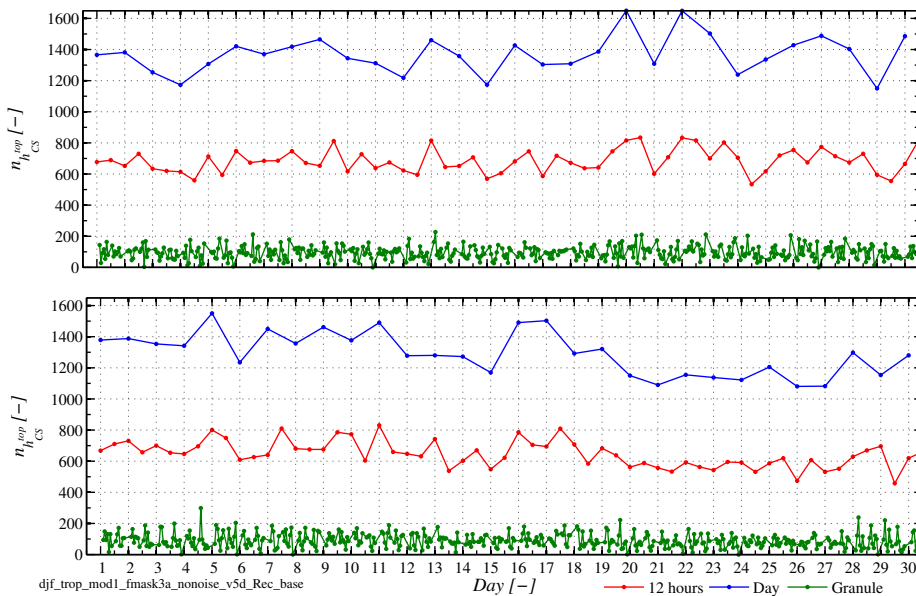


Figure 3.9: Time series of sample number of CloudSat-derived CTH for the period from 1 to 30 January 2007. Each line refers to the time window stepping indicated in the legend. Top panel is for observations at mid-latitudes South (30°S-60°S), and bottom panel uses observations in the tropics (30°S-30°N).

4 Conclusions

Time series of CloudSat observations have been compared to their model equivalent. The analysis has shown that, subject to a quality control screening, there is a reasonable degree of consistency between simulated reflectivity and observations. The extra information brought by the forecast model can be exploited to reduce the size of the minimum anomaly that could be detected through the continuous monitoring of the temporal evolution of statistical parameters derived by the observations. Similar conclusions can be drawn when using reflectivity-derived CTH as monitoring variable since the study has shown that there is a remarkable agreement between observed and simulated CTH.

Given the good agreement between the model FG and observations, a warning system can be put in place where a set of thresholds can be defined for the monitoring quantities that are small enough to be used as checking limits in a warning system. The investigation of CloudSat monitoring possibilities will continue in WP-3100, where the monitoring/warning system will be used to understand the minimum identifiable amplitude of possible anomalies in the radar signal.

Acknowledgements

The NASA CloudSat Project is kindly acknowledged for providing the CloudSat data. Thanks are due to Anton Beljaars and Stephen English for helpful advice and review of the document.

List of Acronyms

CloudSat	NASA's cloud radar mission
CPR	Cloud Profiling Radar
CTH	Cloud Top Height
EarthCARE	Earth, Clouds, Aerosols and Radiation Explorer
ECMWF	European Centre for Medium Range Weather Forecasts
ESA	European Space Agency
FG	First Guess
GCM	Global Circulation Model
IFS	Integrated Forecasting System of ECMWF
NASA	National Aeronautics and Space Administration
NWP	Numerical Weather Prediction
PDF	Probability density function
PSD	Particle Size Distribution
QuARL	Quantitative Assessment of the operational value of space-borne Radar and Lidar measurements of cloud and aerosol profiles
RMSE	root mean square error
SMOS	Soil Moisture and Ocean Salinity mission
SNR	Signal-to-Noise ratio
STSE	Support-to-Science-Element
Z	Radar reflectivity
ZmVar	Z (reflectivity) Model for Variational assimilation of ECMWF

References

- Di Michele, S., M. Ahlgrimm, R. Forbes, M. Kulie, R. Bennartz, M. Janisková, and P. Bauer, 2012: Interpreting and evaluation of the ECMWF global model with CloudSat observations: ambiguities due to radar reflectivity forward operator uncertainties, *Q. J. R. Meteorol. Soc.*, **138**, 2047–2065, doi:10.1002/qj.1936.
- Di Michele, S., E. Martins, and M. Janisková, 2014: Observation operator and observation processing for cloud radar, WP-1100 report for the project Support-to-Science-Element STSE Study - EarthCARE Assimilation, 4000102816/11/NL/CT, ECMWF, 59 pp.
- Hollingsworth, A., D. Shaw, P. Lönnberg, L. Illari, K. Arpe, and A. Simmons, 1986: Monitoring of observation and analysis quality by a data assimilation system, *Mon. Weather Rev.*, **114**, 861–879.
- Janisková, M., O. Stiller, S. Di Michele, R. Forbes, J.-J. Morcrette, M. Ahlgrimm, P. Bauer, and L. Jones, 2010: QuARL - Quantitative Assessment of the Operational Value of Space-Borne Radar and Lidar Measurements of Cloud and Aerosol Profiles, ESA Contract Report on Project 21613/08/NL/CB, 329 pp.
- Muñoz Sabater, J., M. Dahoui, P. de Rosnay, and L. Isaksen, 2012: ESA/ESRIN Contract 4000101703/10/NL/FF/fk Technical Note Phase II, WP1100: SMOS Monitoring Report. Number 2: Nov 2010 - Nov 2011, Technical Report, ECMWF.
- Stephens, G., D. Vane, R. Boain, G. Mace, K. Sassen, Z. Wang, A. Illingworth, E. O'Connor, W. Rossow, and S. Durden, 2002: The CloudSat mission and the A-train, *Bull. Am. Meteorol. Soc.*, **83**(12), 1771–1790.
- Winker, D., M. Vaughan, A. Omar, Y. Hu, K. Powell, Z. Liu, W. Hunt, and S. Young, 2009: Overview of the CALIPSO mission and CALIOP data processing algorithms, *J. Atmos. and Ocean. Tech.*, **26**(7), 2310–2323.